

## Stability and transformations of domain walls in cylindrical wires

Ksenia A. Chichay<sup>1,a</sup>, Igor S. Lobanov<sup>1,b</sup>, Valery M. Uzdin<sup>1,c</sup>

<sup>1</sup>Department of Physics, ITMO University, St. Petersburg, Russia

<sup>a</sup>ks.chichay@gmail.com, <sup>b</sup>lobanov.igor@gmail.com, <sup>c</sup>v.uzdin@mail.ru

Corresponding author: K. A. Chichay, ks.chichay@gmail.com

PACS 75.60.Ch, 75.30.Gw

**ABSTRACT** For magnetic wires and other systems with cylindrical symmetry, algorithms have been proposed for constructing a multidimensional energy surface, searching for minimal energy paths between locally stable states and the activation energies of transitions between such states. The mechanisms of nucleation and transformation of domain walls of various types in amorphous ferromagnetic nanowires with a nonuniform anisotropy distribution have been studied. The stability of the domain walls structure with respect to thermal fluctuations and random external perturbations has been assessed.

**KEYWORDS** Domain wall, cylindrical systems, amorphous ferromagnetic microwires, micromagnetics, domain wall transformation, transition state theory.

**ACKNOWLEDGEMENTS** This work was funded by the Russian Science Foundation (project No. 23-72-10028, <https://rscf.ru/en/project/23-72-10028/>). K.A.Ch. acknowledges the support of ITMO Fellowship Program.

**FOR CITATION** Chichay K.A., Lobanov I.S., Uzdin V.M. Stability and transformations of domain walls in cylindrical wires. *Nanosystems: Phys. Chem. Math.*, 2024, **15** (3), 332–339.

### 1. Introduction

Magnetic wires are among the most suitable and promising systems where creation and controlled movement individual domain walls (DWs) can be used for technological applications such as high-density memory and energy-efficient logic devices [1–3]. A large number of investigations have been devoted to the study of the dynamics of DWs in flat and cylindrical wires. This was stimulated in particular by the concept of a magnetic racetrack memory [2, 4, 5] which requires high speed and high stability of the DW. From this point of view, cylindrical wires as hosts of DW-magnetic bits have a number of significant advantages. DW velocities that have been reported for cylindrical wires reach several kilometers per second [6–9]. Also, due to cylindrical symmetry, there is no preferred direction in the wire perpendicular to the direction of DW movement, and therefore the DW can be oriented at any angle while moving without changing the internal structure, which gives it more stability comparing to DW in planar wires [10, 11].

Very high values of the DW velocity were reported in glass coated amorphous ferromagnetic wires of micron and submicron thickness [8, 12]. Due to the peculiarities of the production process, this type of cylindrical wires have a complex anisotropy distribution induced by internal mechanical stresses [13, 14]. The presence of induced anisotropy in amorphous ferromagnetic wire makes it possible to change their magnetic properties and characteristics of the DW dynamics in a wide range by changing the thickness of the glass shell, fabrication conditions and using various post-processing methods, such as annealing [12, 15]. This makes amorphous ferromagnetic wires in glass shell unique systems with remarkable properties important for applications.

Most of the experimental data are related to the study of the dynamics of the DW and methods for tuning it. However, there is not much information about the type and internal structure of the DWs. The study and description of the local magnetic structure (internal structure of the DW) in microwires is a complex task, which is the flip side of their uniqueness and outstanding properties due to the presence of a complex stress distribution, glass shell, amorphous state and their micrometer size [16]. Previously, we discovered two types of DWs in cylindrical wires with inhomogeneous anisotropy: transverse and radial DWs [17]. But the existence of various types of DWs poses new challenges, since the trend towards miniaturization of the functional elements of devices leads to the problem of their stability with respect to thermal fluctuations and random external disturbances [18, 19]. The presence of inhomogeneous anisotropy can affect the stability of the DWs.

In this work, we examine spontaneous transitions between different type of DWs. We are constructing the energy surface of the system and find on it the minimal energy path between states corresponding to different types of DWs, which allows us to find the activation energy for transitions between them. Also we consider the nucleation process of the radial DW from the homogenous ferromagnetic state.

## 2. Model

The total energy of the system includes exchange energy, anisotropy and Zeeman term:

$$E = E_A + E_K + E_B. \quad (1)$$

The exchange energy is given by the integral

$$E_A = \frac{A}{2} \int_{\Omega} [\nabla \mathbf{S}(\mathbf{r})]^2 d\mathbf{r},$$

where  $\mathbf{S}$  is unit magnetization vector,  $A$  is the exchange stiffness, and the integral is taken over the cylinder representing the cylindrical wire:

$$\Omega = \{0 \leq z \leq L, 0 \leq \rho \leq R, 0 \leq \phi < 2\pi\},$$

where  $\rho, \phi$  and  $z$  are the cylindrical coordinates, with the basic vector  $\mathbf{e}_z$  oriented along the cylinder axis. Energy of anisotropy with constant  $K_i$  and the anisotropy axis  $\mathbf{e}_i$  is given by:

$$E_{K,i} = - \int_{\Omega} K_i(\mathbf{r})(\mathbf{S}(\mathbf{r}) \cdot \mathbf{e}_i)^2 d\mathbf{r}.$$

In cylindrical wire  $\mathbf{e}_i$  may not be constant, but assuming symmetry with respect to rotations around the cylinder axis, the anisotropy can be decomposed over the easy axis/easy plane anisotropies with axes  $\mathbf{e}_\rho, \mathbf{e}_\phi$  and  $\mathbf{e}_z$  oriented along the cylindrical coordinates axes:

$$E_K = E_{K,\rho} + E_{K,\phi} + E_{K,z}.$$

Below, we consider only symmetric case, where anisotropy constants depend only on  $\rho$ .

Zeeman energy for the magnetic field  $\mathbf{B}$  oriented along the cylinder axis has the following form:

$$E_B = -B \int_{\Omega} (\mathbf{S}(\mathbf{r}) \cdot \mathbf{e}_z) d\mathbf{r}.$$

In the simulation we consider the cylinder of finite length  $L$ , hence all energies are bounded, and energy of the homogeneous ferromagnetic state

$$E_{FM} = -(K + B)\pi LR^2.$$

The geometry of the wire plays an important role, for example. in a cylindrical wire, there is no energy barrier for moving the transverse domain wall, while in a rectangular wire, the barrier is non-zero. Commonly used discretization with cubic grid, e.g. in the popular MuMAX3 code, [20] does not allow boundary conditions to be properly taken into account. Codes based on finite element methods, such as [21,22], can correctly work with complex geometry, but the codes are not in public domain and are tricky to implement. For the study we derived discretized energy for the cylindrical domains, which explicitly takes into account the symmetry of the problem and gives precise value for the preferred FM state and error of order  $h^2$  for every smooth magnetization field, where  $h$  is the discretization lattice constant (see Appendix).

In the article we used uniform lattice in the cylindrical coordinates with grid steps:

$$h_\rho = \frac{R}{N_\rho}, \quad h_\phi = \frac{2\pi}{N_\phi}, \quad h_z = \frac{L}{N_z - 1},$$

where  $N_\rho \times N_\phi \times N_z$  is size of the grid. Then the magnetization is defined by array  $n$  of its values at the grid points:

$$\mathbf{S} = \mathbf{S}(\rho, \phi, z), \quad \mathbf{n}_{ijk} = \mathbf{S}(h_\rho(i + 1/2), h_\phi j, h_z k). \quad (2)$$

We use central finite differences to approximate the partial derivatives, which result in staggered grids. To find values of the integrals, we use midpoint and trapezoidal rule, which is appropriated for each term. As the result, we obtain the following discrete forms of the energy contributions. The exchange energy is split into three parts  $E_A = I_\rho + I_\phi + I_z$ , each corresponds to the partial derivatives along the respective coordinate according to the exchange energy integral in the cylindrical coordinates:

$$E_A = \int_{\Omega} \frac{A}{2} \left[ \left( \frac{\partial \mathbf{S}}{\partial \rho} \right)^2 + \frac{1}{\rho^2} \left( \frac{\partial \mathbf{S}}{\partial \phi} \right)^2 + \left( \frac{\partial \mathbf{S}}{\partial z} \right)^2 \right] \rho \cdot d\rho \cdot d\phi \cdot dz$$

The first discretized term can be thought of as the standard Heisenberg interspin exchange, but the exchange parameter in this case is not constant even if the exchange stiffness and magnetization do not change, since the discrete parameter includes non-constant volumes associated with the magnetic element:

$$I_\rho = -h_z h_\phi A \sum_{k=0}^{N_z-1} \sum_{j=0}^{N_\phi-1} \sum_{i=0}^{N_\rho-2} (i+1) \xi_{i+1} \zeta_k \mathbf{n}_{i+1,j,k} \cdot \mathbf{n}_{i,j,k}. \quad (3)$$

It is worth noting that grid points lying on the boundary of the domain have smaller associated volumes, which is taken into account by introducing corrections:

$$\zeta_k = 1, \quad 0 < k < N_z - 1, \quad \zeta_0 = \zeta_{N_z-1} = \frac{1}{2}, \quad (4)$$

and another one for the volume element  $\rho d\rho$ :

$$\xi_i = 1 + \frac{1}{8}\delta_{i,1} + \frac{4R - h_\rho}{8(R - h_\rho)}\delta_{i,N_\rho-1}, \quad i = 1 \dots N_\rho - 1. \quad (5)$$

The two remaining terms has similar forms, but describes interaction with different neighbours:

$$I_\phi = -\frac{h_z}{h_\phi} A \sum_{k=0}^{N_z-1} \sum_{j=0}^{N_\phi-1} \sum_{i=0}^{N_\rho-1} \frac{\zeta_k}{i + 1/2} \mathbf{n}_{i,j,k} \cdot \mathbf{n}_{i,j+1,k}. \quad (6)$$

Here arithmetic with respect to  $j$  is done modulo  $N_\phi$ , since period boundary conditions in  $\phi$  are assumed:

$$I_z = -\frac{h_\phi h_\rho^2}{h_z} A \sum_{i=0}^{N_\rho-1} \sum_{j=0}^{N_\phi-1} \sum_{k=0}^{N_z-2} (i + 1/2) \mathbf{n}_{i,j,k} \cdot \mathbf{n}_{i,j,k+1}. \quad (7)$$

The discretized anisotropy energy and the Zeeman energy are written as

$$E_{K,i} = K_i h_\rho^2 h_\phi h_z \sum_{l=0}^{N_\rho-1} \sum_{j=0}^{N_\phi-1} \sum_{k=0}^{N_z-1} (l + 1/2) \zeta_k (\mathbf{n}_{ljk} \cdot \mathbf{e}_i)^2, \quad (8)$$

and

$$E_B = B h_\rho^2 h_\phi h_z \sum_{i=0}^{N_\rho-1} \sum_{j=0}^{N_\phi-1} \sum_{k=0}^{N_z-1} (i + 1/2) \zeta_k (\mathbf{n}_{ijk} \cdot \mathbf{e}_z). \quad (9)$$

In what follows the exchange stiffness  $A = 2 \cdot 10^{-11}$  J/m, saturation magnetization  $M_s = 500$  kA/m and anisotropy constants  $K_i$  are taken for Fe-based amorphous ferromagnetic wires in glass shell. The sign of  $K_i(\rho)$  defines easy-axis/easy-plane anisotropy, which is non-uniform along the radius  $\rho$  of the wire. The anisotropy axis  $\mathbf{e}_i$  is assumed to be different in the center of the wire, where it coincides with the  $z$  axis  $\mathbf{e}_z$ , and near the surface, where it is assumed to be radial. This partition corresponds to a simplified form of the stress-induced anisotropy distribution in amorphous ferromagnetic microwires in a glass shell, given in Ref. [13, 23]. Thus, starting from the center of the wire to  $0.9R$ , we used the average value of the axial anisotropy  $K_{ax} = 3 \cdot 10^4$  J/m<sup>3</sup> (easy axis). On the periphery, the radial type of anisotropy,  $K_\rho = 2 \cdot 10^4$  J/m<sup>3</sup>, prevails (easy axis). Besides the stress-induced anisotropy, the system contains the effective shape anisotropy for cylinder  $K_{eff} = \mu_0 M_s^2 / 4$  due to the demagnetization fields.

We performed the micromagnetic simulations using own original code, which implements the finite-difference discretization scheme described above. For calculations we used the cylindrical coordinates, taking into account the different volume of units cells to calculate the magnetic moment. The simulated wire was of radius  $R = 1 \cdot 10^{-7}$  m and length  $L = 3.5 \cdot 10^{-7}$  m in case of DW transformation modeling and  $L = 7.5 \cdot 10^{-7}$  m for investigation of nucleation process. Periodic boundary conditions were used in the  $z$  direction. The number of nodes along the each axis was:  $N_\rho = 30$  (from the center of wire to the periphery),  $N_\phi = 100$ ,  $N_z = 140$  or  $N_z = 300$  when considering the transformation or nucleation processes, respectively.

### 3. Domain wall transformation and nucleation

The stability of magnetic domain walls of various types can be studied within the framework of the transition state theory for magnetic degrees of freedom. For this purpose, the energy of the system is considered as a functional of all variables that uniquely determine the magnetic state. This defines the multidimensional energy surface of the system. If a micromagnetic model with a continuous magnetization distribution is used, then the system is divided into cells, each of which has its own size and effective exchange and anisotropy parameters. Local minima on the energy surface are correspond to the ground and metastable magnetic states of the system.

In the cylindrical wires under consideration, the ground state corresponds to a magnetization distribution that does not change along the wire axis. Domain boundaries of various types are metastable states. To find the energy barrier between states corresponding to domain boundaries of different types, a minimum energy path (MEP) between states is constructed. The difference between maximal energy along the MEP and, in the initial equilibrium state, determines the activation energy of the corresponding transition. The path itself corresponds to the most likely transition scenario among nearby paths. In the harmonic approximation, for the dependence of energy on all degrees of freedom at the minimum and saddle point, one can obtain the transition frequencies. The lifetime of the magnetic state at arbitrary temperature can be found if transition in all possible metastable states as well as to the ground state will be taken into account. However, the main role is usually played by the transition with minimal activation energy.

A schematic representation of a cylindrical wire in the cylindrical coordinates is shown in Fig. 1a. In this study, we consider two types of domain walls that are stabilized in a cylindrical wire with inhomogeneous anisotropy, namely radial and transverse domain walls. We described these types of domain walls in more detail in [17].

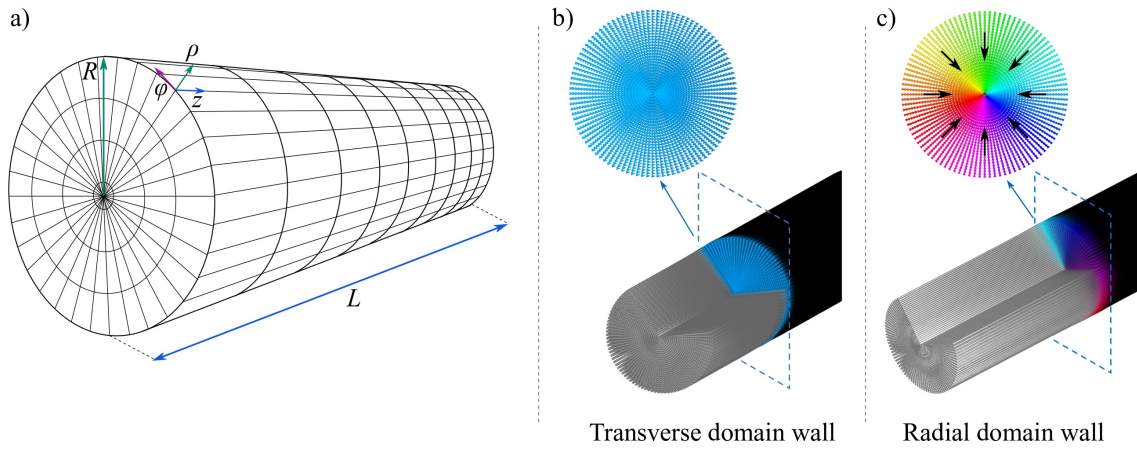


FIG. 1. a) Schematic representation of a wire in the cylindrical coordinate system.  $R$  is the wire radius,  $L$  is the length of the wire. b) and c) 3D view and cross section of the cylindrical wire representing magnetic configuration of transverse DW (b), radial DW (c).

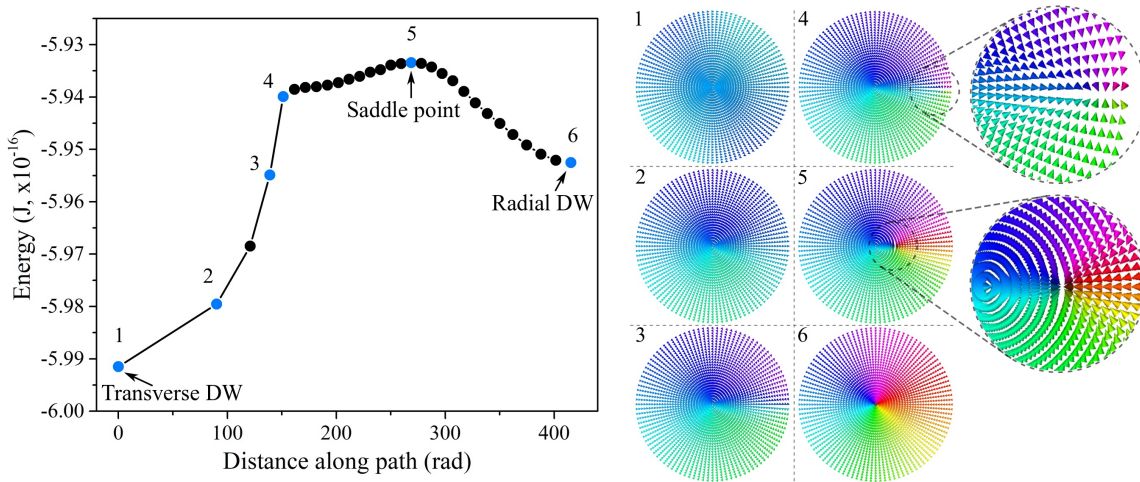


FIG. 2. MEP for the transformation of transverse DW into radial DW in cylindrical wire with inhomogeneous anisotropy. The numbered points on the graph correspond to the magnetic configurations presented on the right side of the figure. Scaled-up parts of magnetic states numbered 4 and 5 correspond to the appearance and propagation of the Bloch point.

Within the framework of the transition state theory, the MEP was calculated for the transformation of a transverse domain wall (designated by number 1 in Fig. 2) into a radial domain wall (designated by number 6 in Fig. 2). It corresponds to the most likely transition scenario among nearby paths and sets the value of the energy barrier shown in Fig. 2. The maximum energy along the path is achieved at the saddle point of the energy surface (configuration number 5 in Fig. 2), and the value of the energy barrier is determined as the difference in energy at the saddle point and the initial equilibrium state corresponding to the chosen structure of the domain wall. The energy barrier value is  $E_{tr} = 5.8 \cdot 10^{-18} J$  for the transition of the transverse DS to the radial one. It can be seen that the transition from a transverse domain wall to a radial one occurs due to the formation of a Bloch point in the peripheral part of the wire and its gradual movement towards the center of the wire. The saddle point in this case (which has the highest energy along the MEP), is the state in which the Bloch point approaches the middle of the wire.

In addition to DW transformation, we also studied nucleation processes of the transverse DW. Magnetization reversal by the rapid DW movement in amorphous ferromagnetic wires in glass shell is characteristic of magnetically bistable wires (which is manifested in a rectangular hysteresis loop). This means that when a new domain nucleates in the middle of the wire, a pair of DW arise, which then immediately propagate in different directions along the axis of the wire.

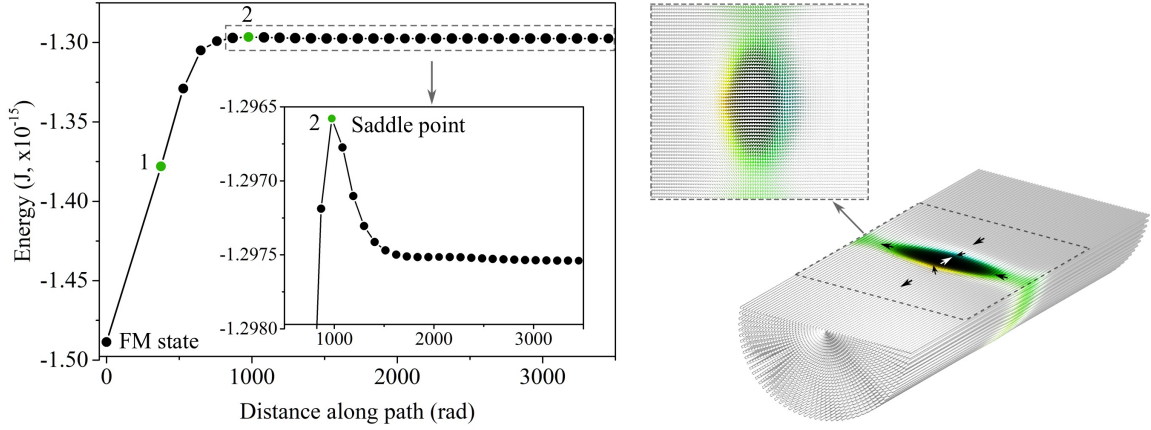


FIG. 3. MEP for nucleation of transverse DWs pair from ferromagnetic state. The right side of the figure depicts the magnetic state corresponding to point 1 on the graph. Point 2 is the saddle point. White and black colors correspond to magnetization along the wire axis.

Therefore, to study nucleation processes, we considered the appearance of two DWs in the middle of the wire and their gradual propagation. Fig. 3 shows the energy barrier for the nucleation of a pair of transverse DWs from the ferromagnetic state. The right side of Fig. 3 corresponds to point 1 on the graph. From this figure, it can be seen that a domain with opposite magnetization begins to nucleate in the center of the wire (indicated in black); thus the DWs are separated in the middle part and merged in the peripheral part of the wire. Subsequently, the formed domain walls separate and move in opposite directions. The value of the energy barrier for nucleation of a pair of transverse DWs is  $E_n = 1.92 \cdot 10^{-16}$  J for a wire with the considered geometric parameters.

#### 4. Conclusion

Construction of the energy surface of magnetic systems and the MEPs between states makes it possible to assess the stability of magnetic states with respect to thermal fluctuations and random external perturbations. The MEP determines the most likely scenario for the transition between different types of DWs and the energy barrier for the activation of such processes. When going from microwires to nanowires, the barrier decreases, which makes transitions between different types of DWs possible at room temperature. The barrier to DW formation and collapse remains sufficiently large, which allows the use of DW to store information in magnetic memory technologies.

#### 5. Appendix

We use a cylindrical grid with grid points located at the intersection of the coordinate surfaces

$$\rho_i = h_\rho(i + 1/2), \quad \phi_j = h_\phi j, \quad z_k = h_z k,$$

where

$$i = 0 \dots, N_\rho - 1, \quad j = 0 \dots, N_\phi - 1, \quad k = 0 \dots, N_z - 1.$$

The values of  $\mathbf{S}$  at the grid points are given by the array  $\mathbf{n}$  defined by (2). The boundary conditions with respect to the polar angle  $\phi$  are naturally periodic, hence

$$\mathbf{n}_{i,0,k} = \mathbf{n}_{i,N_\phi,k}.$$

The boundary conditions on the surfaces  $z = 0$  and  $z = L$  are fixed, since we consider single DW inside the simulation domain, and the deviation of the DW from the FM state is rapidly vanishing:

$$\mathbf{n}_{i,j,0} = \mathbf{e}_z, \quad \mathbf{n}_{i,j,N_z-1} = -\mathbf{e}_z.$$

Due to the continuity of  $\mathbf{S}$ , the value  $\mathbf{S}$  does not depend on  $\phi$  for  $\rho = 0$ , therefore it does not carry a lot of information. Hence the set of grid points  $\rho_i$  do not contain extreme values for the integration domain, while grid points for other degrees of freedom  $\phi$  and  $z$  do.

Partial derivatives are approximated by central finite difference quotients resulting in a staggered grid, that is the field  $\mathbf{S}$  and its derivatives are defined at different points. The derivative with respect to  $z$  is defined only at the centers  $z_{k+1/2}$  of the segments  $[z_k, z_{k+1}]$ :

$$\frac{\partial \mathbf{S}}{\partial z}(\rho_i, \phi_j, z_{k+1/2}) = h_\rho^{-1}(\mathbf{n}_{i,j,k+1} - \mathbf{n}_{i,j,k}) + O(h_z^2).$$

Due to periodic boundary condition with respect to  $\phi$ , the corresponding derivative is defined at  $N_\phi$  points shifted to half lattice constant:  $\phi_j = \phi_j + h_\phi/2$ :

$$\frac{\partial \mathbf{S}}{\partial \phi}(\rho_{i+1/2}, \phi_{j+1/2}, z_k) = h_\rho^{-1}(\mathbf{n}_{i,j+1,k} - \mathbf{n}_{i,j,k}) + O(h_\phi^2).$$

The central finite quotient are readily gives the derivative with respect to  $\rho$  at points  $\rho_{i+1/2} = (i+1)h_\rho$ :

$$\frac{\partial \mathbf{S}}{\partial \rho}(\rho_{i+1/2}, \phi_j, z_k) = h_\rho^{-1}(\mathbf{n}_{i+1,j,k} - \mathbf{n}_{i,j,k}) + O(h_\rho^2).$$

The derivative is not defined at the surface  $\rho = R$  corresponding to  $i = N_\rho$ , but it can be extrapolated to the points using linear extrapolation with the nodes  $\rho_{N_\rho-1}, \rho_{N_\rho-2}$ , which introduce the error term  $O(h_\rho)$ .

The integrals for all the contributions to energy can be written as iterated integrals with respect to the variables  $\rho \in [0, R]$ ,  $\phi \in [0, 2\pi]$  and  $z \in [0, L]$ . We approximate each of the integrals by a numerical quadrature. Namely, we use the trapezoidal rule, if the integrand is given at the ends of the intervals  $[x_k, x_{k+1}]$ :

$$\int_a^b f(x)dx = \sum_{n=0}^N f(x_k)h_x \zeta_n + O(h_x^3),$$

where  $\zeta_k$  is defined by (4), and the rectangle rule, if the integrand is given at the centers of the intervals:

$$\int_a^b f(x)dx = \sum_{n=0}^{N-1} f(x_{k+1/2})h_x + O(h_x^3),$$

where  $x$  is either  $\rho$ ,  $\phi$  or  $z$ . The factors  $\sigma_k$  indicate which fraction of the volume surrounding the point  $x_k$  in the computation grid belongs to the integration domain. Although trapezoid rule is based on linear interpolation of the integrand, while rectangle rule uses only constant interpolation, both rules give the same precision since the term  $x$  is canceled out after integration over any symmetric interval.

To compute integral

$$I_\rho = \frac{J}{2} \int_0^L dz \int_0^{2\pi} d\phi \int_0^R \left( \frac{\partial S}{\partial \rho} \right)^2 \rho d\rho,$$

we use trapezoid rule for the variables  $\phi$  and  $z$ , where the integral with respect to  $\phi$  is taken over the segment  $[0, 2\pi]$  and its ends coincide due to periodic boundary conditions, and rectangle rule for  $\rho$  in the interval  $[\rho_0, \rho_{N-1}]$ . To approximate the integral in the remaining segments  $[0, \rho_0]$  and  $[\rho_{N-1}, R]$ , we assume that the derivative  $\partial \mathbf{S}/\partial \rho$  is constant in the intervals and equal to its values in  $\rho_0$  and  $\rho_{N-1}$ , respectively. This gives us correction terms  $\xi_i$  (see (5)) to the rectangle rule for the first and the last segments. Thus, the expression (3) is obtained.

The quadrature for the exchange integral

$$I_\phi = \frac{J}{2} \int_0^L dz \int_0^R \frac{d\rho}{\rho} \int_0^{2\pi} \left( \frac{\partial S}{\partial \phi} \right)^2 d\phi,$$

is obtained using the rectangle rule for the integral with respect to  $\phi$  with points  $\phi_{j+1/2}$  (taking into account periodic boundary conditions), the trapezoid rule for  $z$  and the rectangle rule for  $\rho$  with grid points  $\rho_i$ . It is worth noting that we consider only smooth magnetization fields, therefore the derivative under the integral is zero at the origin and the integral does not have singularities. The final quadrature is given by (6).

The third exchange integral

$$I_z = \frac{J}{2} \int_0^R \rho d\rho \int_0^{2\pi} d\phi \int_0^L \left( \frac{\partial S}{\partial z} \right)^2 dz$$

is obtained using the same rule for  $\rho$  as in  $I_\phi$ , the same rule for  $\phi$  as in  $I_\rho$ , and rectangle rule for the integral over  $z$  with grid points  $z_{k+1/2}$ . The quadrature formula obtained is given by (7).

The anisotropy energy contributions

$$E_K = \sum_l K_l \int_0^R \rho d\rho \int_0^{2\pi} d\phi \int_0^L (\mathbf{S} \cdot \mathbf{e}_l)^2 dz,$$

and the Zeeman energy contributions

$$E_B = B \int_0^R \rho d\rho \int_0^{2\pi} d\phi \int_0^L (\mathbf{S} \cdot \mathbf{e}_z) dz,$$

are approximated by using the trapezoid rule for integrals with respect to  $\phi$  and  $z$  (with periodic BC for  $\phi$ ), and the rectangle rule for the integral with respect to  $\rho$ . The corresponding quadratures are (8), (9).

The proposed discretization scheme gives an exact answer for linear functions  $\mathbf{S}$  in precise arithmetic. Among the functions only constant ones satisfy the constraint on the length of the magnetization, hence the exact answer is obtained only on the ferromagnetic state. In all other magnetization fields, the error of the provided quadrature formulas for the contributions to energy equals  $O(h^2)$ , which is originated from extrapolation of  $\partial S/\partial \rho$  to the ends of integration interval in computation  $I_\rho$ .

We benchmarked the convergence of the discrete model to the micromagnetic one using domain wall ansatz

$$\mathbf{S} = (\sin \theta \cos \phi, \sin \theta \sin \phi, \cos \theta),$$

where  $\phi$  is an arbitrary fixed angle, and

$$\theta(z) = 2 \arctan \exp \frac{z}{\Delta},$$

with DW width  $\Delta = 1.36 \cdot 10^{-8}$  m. The magnetic wire geometry and parameters were the same as in the main part of the article. The sparsest grid has size  $N_\rho = 2$ ,  $N_\phi = 2$ ,  $N_z = 8$ . The step sizes for all the dimensions were scaled with the same factor, gradually increasing resolution of the boundary. The total exchange energy error compared to the micromagnetic one scales as  $O(h^2)$  as expected. Anisotropy energy error decreases even faster as step size decreases, since the term does not suffer from the extrapolating procedure. For comparison, we computed energy of the same ansatz using Mumax3 [20] (Fig. 4). The cubic grid used in Mumax3 can not approximate surface of the cylinder reasonable well, resulting in highly nonmonotonic convergence and 6 orders of magnitude larger errors for the anisotropy energy and 1 order for the exchange energy.

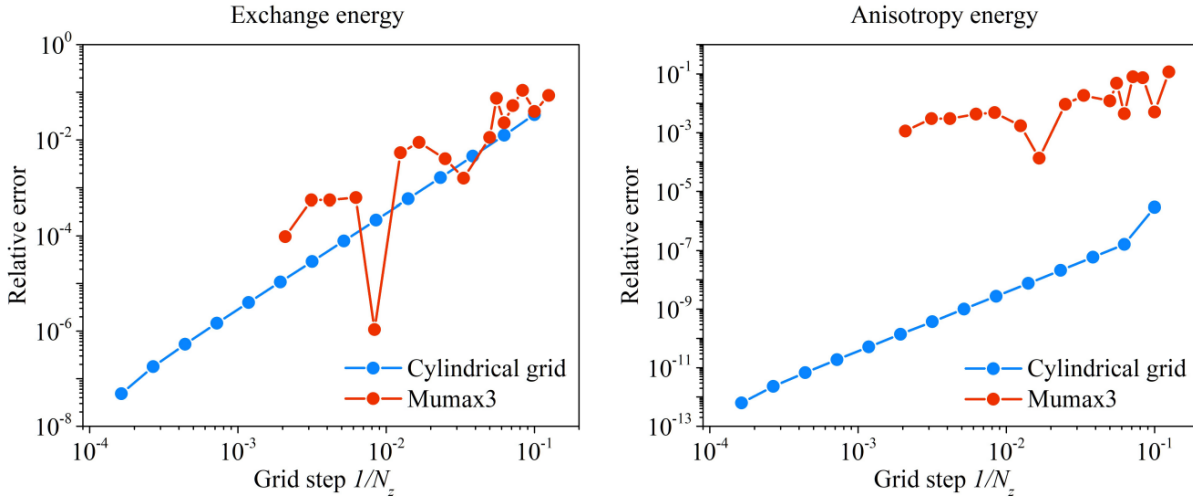


FIG. 4. Relative error for exchange and anisotropy energies for transverse DW computed in discrete models as a function of the grid step  $h_z$ . (Blue line) Energy estimated by (3), (6), (7) and (8). (Red line) Energy computed using Mumax3.

## References

- [1] Foerster M., Boule O., Esefelder S., Mattheis R., Kläui M. *Domain Wall Memory Device*. In: Xu, Y., Awschalom, D., Nitta, J. (eds) Handbook of Spintronics. Springer, Dordrecht, 2016
- [2] Parkin S.S.P., Hayashi M. and Thomas L. Magnetic Domain-Wall Racetrack Memory. *Science*, 2008, **320**(5873), P. 190–194.
- [3] Venkat G., Allwood D.A., Hayward T.J. Magnetic domain walls: types, processes and applications. *J. Phys. D: Appl. Phys.*, 2024, **57**, P. 1688.
- [4] Parkin S., Yang S.H. Memory on the racetrack. *Nature nanotechnology*, 2015, **10**(3), P. 195–198.
- [5] Blasing R. et al. Magnetic Racetrack Memory: From Physics to the Cusp of Applications Within a Decade. *Proc. IEEE* 2020, **108**, P. 1303–1321.
- [6] Hertel R. Ultrafast domain wall dynamics in magnetic nanotubes and nanowires. *J. Phys.: Condens. Matter*, 2016, **28**, P. 483002.
- [7] Yan M., Andreas C., Kakay A., Garcia-Sanchez F., Hertel R. Fast domain wall dynamics in magnetic nanotubes: Suppression of Walker breakdown and Cherenkov-like spin wave emission. *Appl. Phys. Lett.*, 2011, **99**, P. 122505.
- [8] Corte-León P., Gonzalez-Legarreta L., Zhukova V., Ipatov M., Blanco J.M., Churyukanova M., Taskaev S. and Zhukov A. Controlling the domain wall dynamics in Fe-, Ni- and Co-based magnetic microwires. *J. Alloys Compound.*, 2020, **834**, P. 155170.
- [9] Tejo F., Fernandez-Roldan J.A.F., Guslienko K., Otxoa R.M. and Chubykalo-Fesenko O. Giant supermagnonic Bloch point velocities in cylindrical ferromagnetic nanowires. *Nanoscale*, 2024, Advance Article
- [10] Alam J., et.al. Cylindrical micro and nanowires: Fabrication, properties and applications. *J. Magn. Magn. Mater.*, 2020, **513**, P. 167074.
- [11] Yan M. Beating the Walker limit with massless domain walls in cylindrical nanowires. *Phys. Rev. Lett.*, 2010, **104**, P. 057201.
- [12] Zhukova V., Corte-Leon P., González-Legarreta, L., Talaat, A., Blanco, J.M., Ipatov, M., Olivera, J. and Zhukov, A. Review of domain wall dynamics engineering in magnetic microwires. *Nanomaterials*, 2020, **10**(12), P. 2407.
- [13] Chiriac H., Ovari T., Zhukov A. Magnetoelastic anisotropy of amorphous microwires. *J. Magn. Magn. Mater.*, 2003, **496**, P. 254–255.

- [14] Zhukova V., Blanco J.M., Ipatov M., Zhukov A. Magnetoelastic contribution in domain wall dynamics of amorphous microwires. *Physica B*, 2012, **407**, P. 1450–1454.
- [15] Chichay K., et. al. Tunable domain wall dynamics in amorphous ferromagnetic microwires. *J. Alloys Compound.*, 2020, **835**, P. 154843.
- [16] Gudoshnikov S.A., Grebenshchikov Yu.B., Ljubimov B.Ya., Palvanov P.S., Usov N.A., Ipatov M., Zhukov A., Gonzalez J. Ground state magnetization distribution and characteristic width of head to head domain wall in Fe-rich amorphous microwire. *Phys. Stat. Sol. A*, 2009, **206**(4), P. 613–617.
- [17] Chichay K.A., Lobanov I.S., Uzdin V.M. The structure of magnetic domain walls in cylindrical nano- and microwires with in- homogeneous anisotropy. *Nanosystems: Phys. Chem. Math.*, 2023, **15**, P. 55–59.
- [18] Lobanov I.S., Potkina M.N., Uzdin V.M. Stability and Lifetimes of Magnetic States of Nano- and Microstructures (Brief Review). *JETP Letters*, 2021, **113**, **12**, P. 801–813.
- [19] Lobanov I.S., Uzdin V.M. The lifetime of micron scale topological chiral magnetic states with atomic resolution. *Comp. Phys. Commun.*, 2021, **269**, P. 108136.
- [20] Vansteenkiste A., Leliaert J., Dvornik M., Helsen M., Garsia-Sanchez F., B. Van Waeyenberge F. The design and verification of MuMax3. *AIP Advances*, 2014, **4**, P. 107133.
- [21] Fischbacher T., Franchin M., Bordignon G., and Fangohr H. A Systematic Approach to Multiphysics Extensions of Finite-Element-Based Micromagnetic Simulations: Nmag, *IEEE Transactions on Magnetics*, 2007, **43**(6), P. 2896–2898.
- [22] Abert C., Exl L., Bruckner F., Drews A., Suess D. magnum. fe: A micromagnetic finite-element simulation code based on FEniCS. *Journal of Magnetism and Magnetic Materials*, 2013, **345**, P. 29–35.
- [23] Chiriac H., Ovari T.A., Pop Gh. Internal stress distribution in glass-covered amorphous magnetic wires. *Phys. Rev. B.*, 1995, **52**(14), P. 10104.

---

*Submitted 10 April 2024; revised 8 May 2024; accepted 11 May 2024*

*Information about the authors:*

*Ksenia A. Chichay* – Department of Physics, ITMO University, St. Petersburg, 197101, Russia; ORCID 0000-0002-6921-6075; ks.chichay@gmail.com

*Igor S. Lobanov* – Department of Physics, ITMO University, St. Petersburg, 197101, Russia; ORCID 0000-0001-8789-3267; lobanov.igor@gmail.com

*Valery M. Uzdin* – Department of Physics, ITMO University, St. Petersburg, 197101, Russia; ORCID 0000-0002-9505-0996; v.uzdin@mail.ru

*Conflict of interest:* the authors declare no conflict of interest.